Analysis of $Fe_{78}Si_9B_{13}$ (%at.) ribbons of noncommercial scrap materials produced by melt spinning equipment

Marcelo R. Pagnola, Mariano Malmoria,
Marcelo Barone and Hugo Sirkin
*Laboratory of Amorphous Solids, INTECIN (UBA-CONICET),
Buenos Aires, Argentina*

Abstract

Purpose – The purpose of this paper is to present a ribbons production route of composition $Fe_{78}Si_9B_{13}$ (%at.) using low cost noncommercial scrap materials to obtain usable magnetic cores by melt spinning technique and their characterization. This way, these may compete with the materials produced by conventional casting processes.

Design/methodology/approach – The methodology is to design a master alloy with scrap different starting compositions, to which Fe is added to get the desired atomic ratio of components. With this starting alloy, using the method of melt spinning, in its variant of chill block melt spinning, are achieved amorphous ribbons with desired soft magnetic behavior. Then these ribbons are thermally treated for achieve nanocrystalline structures to improve the performance in the magnetic cores.

Findings – The result of this paper shows that it is possible to recycle scrap materials, and re-used efficiently as components essential in part of electrical components. This way, these may compete with the materials produced by conventional casting processes.

Research limitations/implications – The limitation of this work to ensure that the scrap materials used is reasonably adequate to accomplish obtaining the master alloy, i.e. having reduced impurities.

Practical implications – The implications are important, because it assures that the components are recyclable and also high-tech in reference to energy saving that involves the production of amorphous and nanocrystalline materials in the electric industry. These products may compete with those produced by conventional casting processes.

Social implications – The social implications lead to awareness in recycling and energy saving as an option for social progress in technology.

Originality/value – The originality of the study is that it takes as a starting point for the final product (ribbon) noncommercial scrap materials of known composition and the obtained results are comparable to those that also are manufactured from the pure elements. The control of impurities is necessary in the production route. This way, these may compete with the materials produced by conventional casting processes. This process achieved a production with lower cost, high efficient energy products and high added value.

Keywords Amorphous materials, Magnetic materials, Magnetic ribbons, Mossbauer effect, Nanostructures

Paper type Research paper

1. Introduction

The present application range of available soft magnetic materials has been significantly increased by the development of amorphous, bulk metallic glasses and nanocrystalized systems (Lavorato *et al.*, 2011). These ferromagnetic alloys can be obtained as glassy phases by the rapid cooling technique; some of them partially crystallize by certain heat treatment achieving structures composed by ten to 40 nanometer long grains surrounded by a glassy phase (Kim *et al.*, 2013; Švec *et al.*, 2003). These materials are

used in the manufacturing of electric transformer cores showing meaningful improvement on its overall outputs as an increment in the efficiency and less environmental impact. In the past, these cores have been produced with grain-oriented electrical steel and nongrain-oriented electrical steel, ferrite, Ni-Fe and Co-Fe alloys strips produced by conventional casting processes, which requires several mechanical and thermal manufacturing techniques, some of them of high cost (Gelinas *et al.*, 2000). The new manufacture of nanostructured magnetic products can be done by the direct use of the ribbons obtained by melt-spinning process and post-melt spinning heat treatments; adjusting the width of the ribbon through the nozzle's design. The success of the ribbon's formation significantly depends on how the nozzle design affects the melt's flow (Olofinjana *et al.*, 2004; Bedell *et al.*, 1987; Kurokawa *et al.*, 1999) used during the casting process. Furthermore, the magnetic products used can be extended to complex geometries introducing a milling stage afterwards the melt-spinning process to obtain refined elemental powder particles (Nowacki *et al.*, 2006; Byoung-Gi, *et al.*, 2007; Dobrzanskia *et al.*, 2004), which by a metallurgical process give us the desired product.
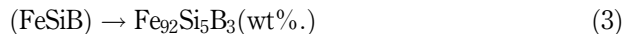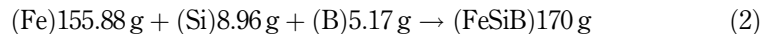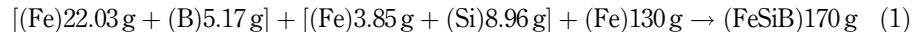
Our researches and other authors confirm that energy losses in magnetic cores uncharged can be reduced almost 80 percent from those that appear in devices built with traditional steel (De Cristofaro, 1998; Muraca *et al.*, 2009).

In this work, $Fe_{78}Si_9B_{13}$ (%at.) ribbons are produced from a mother ingot previously melted from noncommercial alloys. These ribbons were cooled on the copper wheel in air atmosphere. The process temperature is controlled by optical pyrometer implemented on a tripod located at the focal distance of one meter from the melted sample (Pagnola *et al.*, 2009; Pagnola and Katabian, 2012).

2. Experimental development
2.1 Mother ingot preparation
An ingot mother (170 g) is obtained by 27.20 g of $Fe_{81}B_{19}$ (%wt.) and 12.80 g of $Fe_{30}Si_{70}$ (%wt.) of noncommercial scrap alloys, and by the addition of 130 g of Fe in the form of granules. With these samples there is obtained an ingot with the following features:

$$[(Fe)22.03\,g + (B)5.17\,g] + [(Fe)3.85\,g + (Si)8.96\,g] + (Fe)130\,g \rightarrow (FeSiB)170\,g \quad (1)$$

$$(Fe)155.88\,g + (Si)8.96\,g + (B)5.17\,g \rightarrow (FeSiB)170\,g \quad (2)$$

$$(FeSiB) \rightarrow Fe_{92}Si_5B_3(wt\%.) \quad (3)$$

Then, we proceeded to melt in vacuum atmosphere the first mother ingot in a specially designed graphite crucible. This procedure used a 7.5 kW induction furnace RDO^{TM} model LFI-7.5 mounted as shown in Figure 1. The equipment is formed by an induction coil inside a vacuum chamber, where inert atmosphere is produced by a vacuum pump for such purpose. This is the ad hoc production equipment installed.

The impurities in the noncommercial scrap alloy are: Al, C, Ca and S. Their quantity is lower than 0.3 %wt.

This procedure is repeated four times for the homogenization of the alloying elements. Using a temperature of 1275°C, which is determined by the phase diagram and the corresponding proportion of the majority binary alloy (SGTE, 2004). This temperature is controlled by an optical pyrometer Micro-Epsilon brand and model CTLM 2HSF300-C3, mounted on a tripod and focussed upon a graphite crucible.
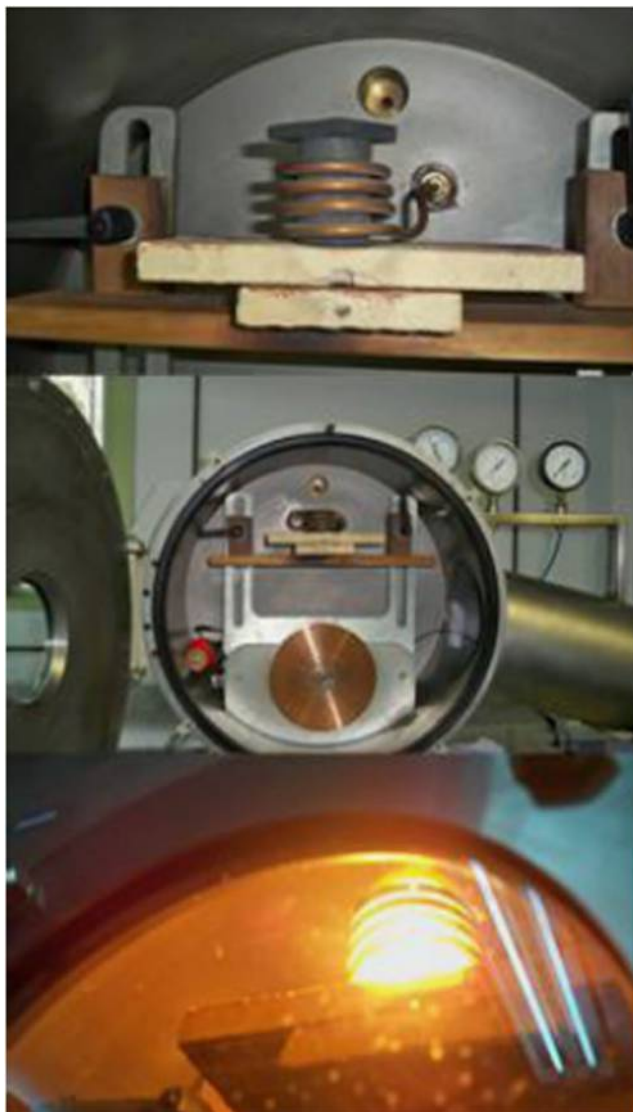
Figure 1.
$Fe_{92}Si_5B_3$ (%wt.), mother
ingot casting process

The ingot was sectioned approximately by its half and the homogeneity control
performed on Fe element was analyzed by Energy Dispersive Spectroscopy (EDS)
technique (EDAX™), considering about 100 measurements (%wt./Mol) on linear paths
of 200 μm on the surface and center sample.

2.2 Obtaining ribbon
The obtained mother ingot was cracked to an average particle size of about 5 mm, and
then placed inside a quartz tube of 10 mm diameter and 1.5 mm thick. This tube works
as crucible for the obtaining ribbon new process. This crucible has a Boron Nitride

nozzle attached with a circular 0.6 mm hole practiced in its center, through which flowing the molten alloy. This is done with ad hoc new disposition in the induction furnace used in Section 2.1 (see Figure 2).

The wheel works as a heat sink reaching around one million degrees per second cooling rate ($\sim 10^6$ K/s) necessary to achieve the glassy phase (Praisner *et al.*, 1995). The obtaining method of ribbons is typically reported through melt spinning process by different authors (Allia *et al.*, 1982; Muraca *et al*, 2009; Wang, 2010). In Figure 2 it is shown the melt spinning equipment, where it can be seen the small gap between ribbon and the casting wheel. The temperature profile is controlled by the external optical pyrometer. The stabilization zone is reached at 7 minutes of warm to the ejection temperature and the ejection is done at 8.9 minutes (Figure 3).

Then, with an induction coil which heats the alloy over the melting point and argon overpressure the alloy is expulsed through the nozzle at ejection velocity on the high speed spinning wheel. As a result, a continuous and mostly amorphous ribbon is obtained. Its thickness and width are determined as a function of the pressure and the gap between the nozzle and the wheel. These parameters are showed in Table I.
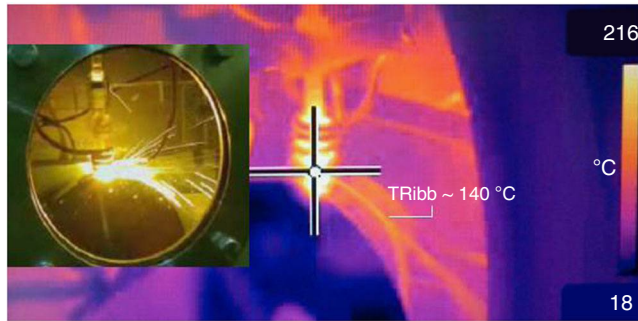
Figure 2.
Air cooling and melting of $Fe_{78}Si_9B_{13}$ (%at.) to obtain ribbon in melt spinning equipment
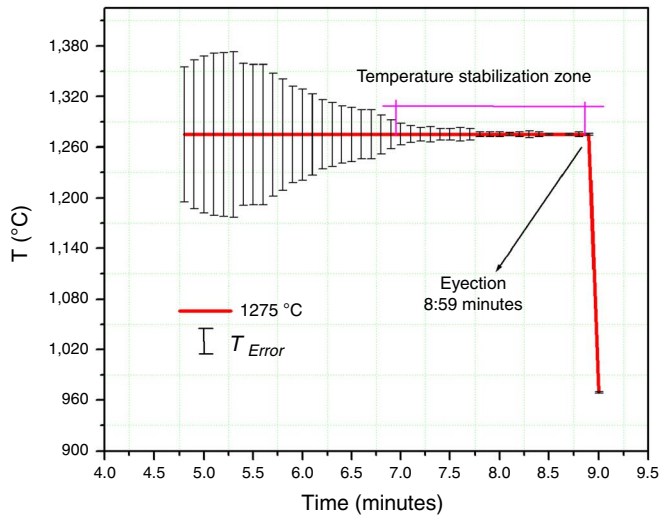
Figure 3.
Temperature stabilization zone controlled by the external optical pyrometer

The values used in the gap are typical to identify this methodology as chill block melt spinning (Pavuna, 1981). This process differs from the planar flow casting, which uses sub-millimeter gaps (Lim *et al.*, 2009).

The obtained ribbon has an average thickness of 32 μm and an average width (A) of 1.18 mm.

Was estimated cooling rate according to Equation (4) (Wang, 2010) in -2.73×10^6 K/s assumed the same composition, whereas at wheel speed (V_x) is according to Table I, the value $x = 2.3 \times 10^{-3}$ m according to the relationship $x/z = 3.8395$, being $z = 0.0006$ m the orifice diameter nozzle:

$$\frac{\partial T}{\partial t} = -156.97 \cdot \left(\frac{Vx}{x}\right) \tag{4}$$

The estimated solidification time is 9.4×10^{-7} s, and was calculated according to Chen *et al.* (2011). For this value, we apply the coefficients from Table II.

The x-ray diffraction analysis (XRD) ingot and ribbon results were performed at room temperature using a Rigaku™ diffractometer with Θ-2Θ configuration and vertical goniometer with CuKα monochromatic radiation (1.54056 Å).

The Calorimetry Differential Scanning Analysis (DSC) on Fe$_{78}$Si$_9$B$_{13}$ (%at.) ribbon was carried out a temperature sweep at a rate of 80 K/min with a Perkin Elmer™, Pyris 1DSC model equipment. The sample was weighed in 5.13 mg and then placed in Cu casserole for comparison with a reference. The sweep was carried out in the temperature range from 200 to 650°C in argon gas controlled atmosphere.

To complete the structure alloys the Mössbauer spectroscopy (MS) analysis was used at room temperature in a ^{57}Fe (50 mCi) sealed source Rh matrix arranged with transmission geometry. The data were fitted with two distributions in the Winnormos2k program. The calibration was done with α-Fe foil and isomer shifts (Is) are given relative to α-Fe.

Speed wheel (m/sec)	Gap (mm)	Ejection pressure (Bar)	
40	3	0.3	Table I. Set up parameters

Parameter	Material Fe$_{78}$B$_{13}$Si$_9$	Copper roller	–		
Initial temperature, T_0 (°C)	1,275 (T_{10})	25 (T_{20})	–		
Thermal conductivity, λ (W/(m °C))	80 (λ_1)	398 (λ_2)	–		
Specific heat capacity, C (J/(kg °C))	553 (C_1)	386 (C_2)	–		
Density, ρ (kg/m^3)	7,500 (ρ_1)	8,930 (ρ_2)	–		
Coefficients of thermal storage, b (W$_{\sqrt{}}$/S/(m^2 °C))	18,215 (b_1)	37,039 (b_2)	–		
Coefcient in Fourier's equation (Wm^2/J)	1.928x10^{-5}	–	–		
Latent heat crystallization, L (kJ/kg)	251 (Fe)	–	1,790.02 (Si)	4,643.84 (B)	
Temperature of the ribbon-roller interface (°C)	437.07				
Eutectic temperature, Te (°C)	1,150	–			
Distance normal to the roller surface (m)	0.003	–	–		

Table II.
Initial conditions values and physical parameters of materials for calculating solidification time according to Chen *et al.* (2011)

The magnetic analysis was performed only over magnetic ribbon through low temperatures hysteresis curves in a Superconducting Quantum Interference Device (SQUID) magnetometer under an applied field of 7 T. There was obtained: saturation magnetization (M_S); remanent magnetization (M_R); and coercivity (H_C) values.

3. Results and discussion

3.1 Ingot EDS analysis

The attributable percentages of Fe element show its homogeneous bulk distribution (see Figure 4). Furthermore, comparing the molar ratios of Fe with the atomic percent (Table III) to the weight of the studied ingot showing excellent distribution of this element designed by Equation (3).
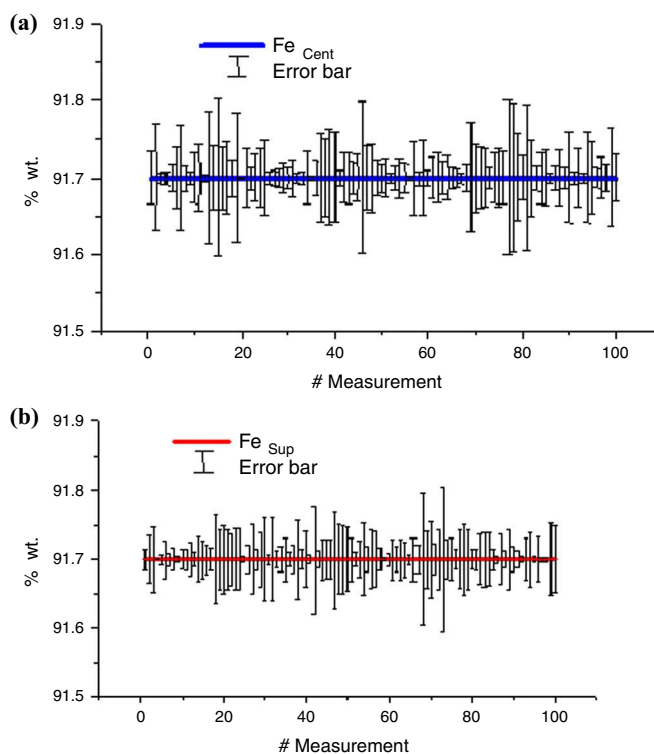

Figure 4.
(a) Fe (%wt.) measurements in sample center. (b) Fe (%wt.) measurements in sample surface

Note: Step is 2 microns per point that is evaluated

| $Fe_{78}Si_9B_{13}$	47.492 g	Wt./mol	Lingote ($\sim$95 g)
Fe	43.56 g	91.7 %wt.	87.1 g
Si	2.527 g	5.3 %wt.	5 g
B	1.405 g	3 %wt.	2.9 g

Table III.
Ingot molar ratio

3.2 XRD
In the ingot diffractogram (Ingot) (see Figure 5) it can be seen the appearance of the crystalline phase (C) F_eSi_2 at the peak (2 1 1) and Fe_2B on the peaks (1 1 0), (2 0 0), (2 2 0), (3 1 0) and (3 3 0), plus Fe element in peaks (1 1 0), and (2 0 0). The phase distribution and suggested elements according to the analysis is:

$$Ingot \rightarrow 0.13(Fe_2B) + 0.045(F_eSi_2) + 0.475(Fe)(\% \text{ at.})(C) \tag{5}$$
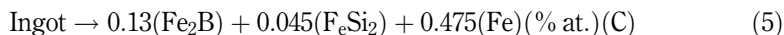
In the ribbon diffractogram (Ribbon) (see Figure 5) it can be observed the angular widening crystalline sites compared to the diffractogram of the crystalline ingot mother alloy $Fe_{92}Si_5B_3$ (%wt.). These results show amorphization in these peaks. Being then, the product obtained by the melt spinning technique mostly amorphous (Am). The nanocrystalline peak was determined (Nc) in (1 2 0), and the amorphous peak (1 4 1) of the peaks SiB_6. The (1 1 0) and (3 1 1) of FeB, and the (1 0 1) and (2 0 0) of $Fe_{0.91}Si_{0.09}$. The distribution phase suggested for the Ribbon is as follows:

$$Ribbon \rightarrow 0.0161(SiB_6)(Nc+Am) + 0.82(Fe_{0.91}Si_{0.09})(Am) + 0.0331(FeB)(Am)(\%at.) \tag{6}$$
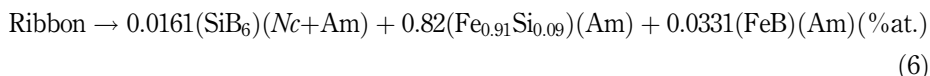
For heat-treated ribbon at 730°C (TT Ribbon), its diffractogram indicates the occurrence of the peaks (1 0 4), (2 1 7) and (1 3 7) of B_β, the peaks (1 0 1) and (2 0 0) $Fe_{0.91}Si_{0.09}$, the peaks (1 2 1), (2 2 0) and (3 1 1) FeB and the $FeSi_2$ (2 1 1) peak. These indicate predominantly nanocrystalline structure (Nc) which suggest the following distribution of phase (Table IV):
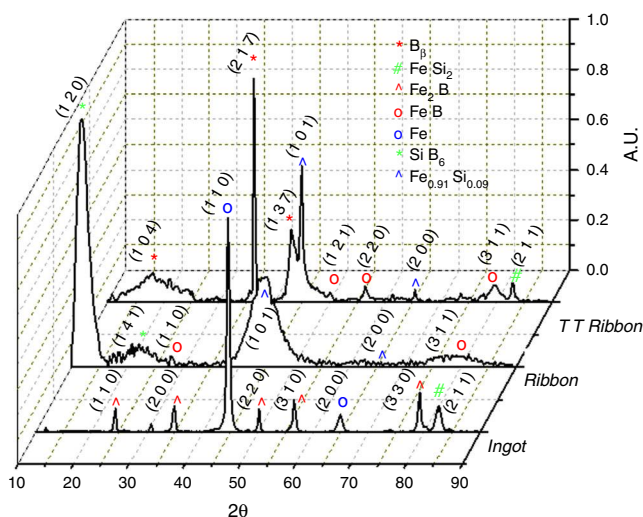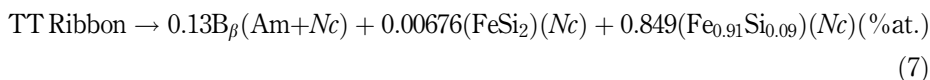
$$TT Ribbon \rightarrow 0.13B_\beta(Am+Nc) + 0.00676(FeSi_2)(Nc) + 0.849(Fe_{0.91}Si_{0.09})(Nc)(\%at.) \tag{7}$$

Figure 5.
Diffractograms comparison $Fe_{92}Si_5B_3$ alloy (%wt.)

The nanocrystals sizes were estimated by the Scherrer ecuation (Equation (8)) (Khorsand Zaka *et al.*, 2012), and are shown in Table V:

$$D = \frac{\kappa.\lambda}{\beta d.\cos(\Theta)} \tag{8}$$

where D is the crystalline size in nanometers, λ is the wavelength of the radiation, k is a constant equal to 0.94, $\beta d = \beta$-0.05 is the peak width at half-maximum intensity whit error instrument, and Θ is the peak position, β is the peak width at half-maximum intensity and 0.05 represent the mean value of the XRD instrument error.

3.3 Calorimetry differential scanning analysis (DSC)
The Figure 6 shows three well-defined stages. The first exothermic event is where secrete mostly the amorphous regions rich in Si and B. From the Curie temperature, $T_{c,am} = 398°C$ occurs a rearrangement by Si atoms diffusion in rich Fe amorphous matrix up before the first transformation peak T_{Fc} (Yardley *et al.*, 2007; Chang and Marti, 1983; Rawers *et al.*, 1988). The second heat release event corresponds to a first crystallization (T_{Fc}) at 593°C, in which the amorphous Si rich region precipitates in a nanocrystalline composite $Fe_{0.91}Si_{0.09}$. The third event corresponds to a second crystallization (T_{Sc}) at 601°C, caused by the increased number of B_{β} and $FeSi_2$ nanocrystals (Sun *et al.*, 2000; Chau *et al.*, 2005).

3.4 MS analysis
In Mossbauer spectra (Ribbon) it was possible to observe two distributions, the first one distribution fits in a 76.11 percent of spectrum's data with a maximum hyperfine

Elements Peaks	PDF Number	Reference
B_{β}	#31-0207	Calvert (1985)
$FeSi_2$	#35-0822	NBS (1985)
Fe_2B	#39-1314	Khan (1988)
FeB	#32-0463	NBS (1981)
Fe	#06-0696	Swanson *et al.* (1955)
SiB_6	#35-0809	NBS (1984)
$Fe_{0.91}Si_{0.09}$	#96 – 900-6909	Zhang and Guyot (1999)

Table IV. Diffractometry identification cards

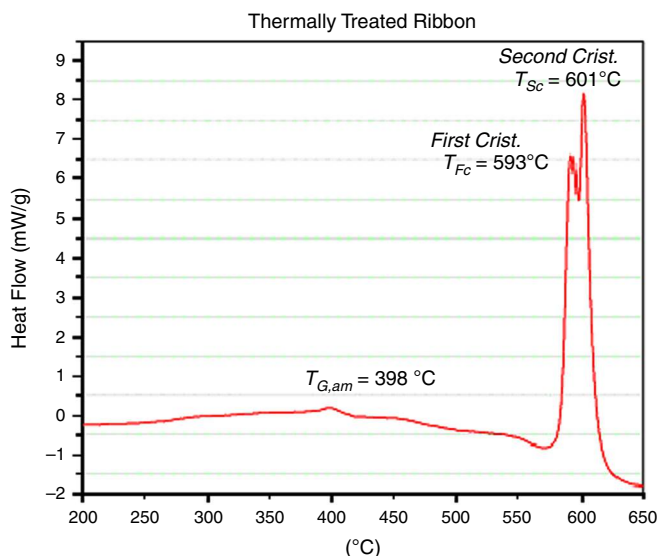| Peek	Scherrer D (nm)
(1 2 0)	3.260
(2 1 7)	23.22
(1 3 7)	21.35
(1 0 1)	23.88
(2 2 0)	11.27
(2 0 0)	14.75
(3 1 1)	6.31
(2 1 1)	18.92

Table V. Nanocrystals sizes

Figure 6.
DSC crystallization
curve of $Fe_{78}Si_9B_{13}$
(%at.) alloy ribbon

field (BHF) at 22.6 T, and Is of 0.3897×10^{-1} mm/s attributable to Fe-rich highly deformed-bcc regions (Kim *et al.*, 2013). The second one distribution adjusts the remaining 23.89 percent of spectrum's data distribution affected by the presence of two peaks: the first with maximum hyperfine field at 12.7 T, the second at 24.7 T and Is is 0.2951 mm/s, attributable to B-centered prismatic regions (Aykol *et al.*, 2009) (Figure 7).

3.5 Magnetic response analysis

The H_C values decreased as the temperature was raised to as: 88.75 Oe (20 K), 20.77 Oe (40 K), 7.46 Oe (60 K). The same phenomenon occurs with M_R values: 22.44 emu/g (20 K), 10.32 emu/g (40 K), 2.56 emu/g (60 K). The M_S values do not vary significantly and are close to 135 emu/g at different temperatures tested as shown in Figure 8. All reported curves follow a soft magnetic material typically nearby to the behavior of the commercial alloys known as FINEMET® a soft magnetic material exhibiting excellent permeability while maintaining a high saturation magnetization (Yoshizawa *et al.*, 1988).

3.6 General discussion

The achieved high cooling rate avoids the total crystallization and the result was an amorphous structure. This was checked by XRD analisys in Section 3.2 and confirmed by MS analysis in Section 3.4 where the 22.6 T hyperfine field peak is close to the reported by Miglierini (1994), and can be attributed to Fe atoms surrounded by Si atoms, in the first distribution. The 24.7 T BHF peak to the remaining 23.89 percent amorphous phase, can be attributed to FeB environments according to Franke *et al.* (1980) also seen in the XRD analysis conclusively in the peak (3 1 1) of FeB, while the remaining 12.7 T peak is attributable environments rich in Si in XRD peaks (1 4 1) and (1 0 1) (Figure 5 – Ribbon). The subsequent process heating to 730°C gives rise to solid solution $Fe_{0.91}Si_{0.09}$ (Nc) (Thongmee *et al.*, 1999; Chacón *et al.*, 2001) also detected in XRD peak (1 0 1) (Figure 5 – TT Ribbon). The amorphous phases observed in diffraction patterns (Figure 5 – Ribbon) are evidenced with a radial distribution
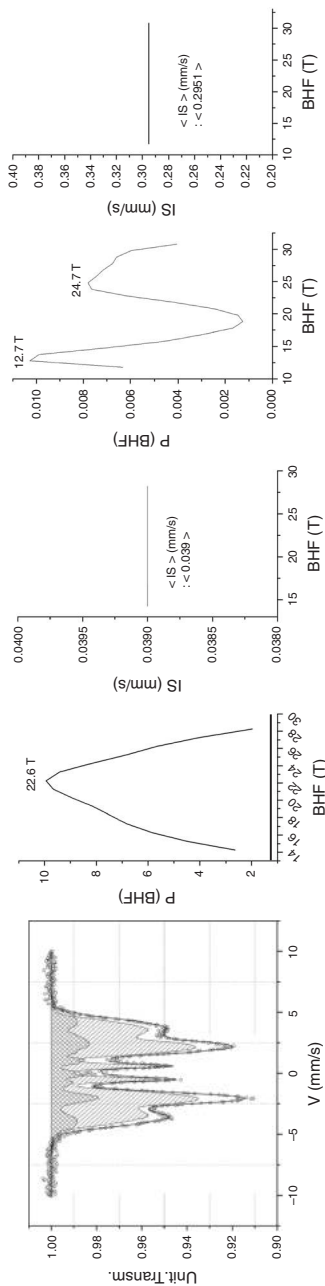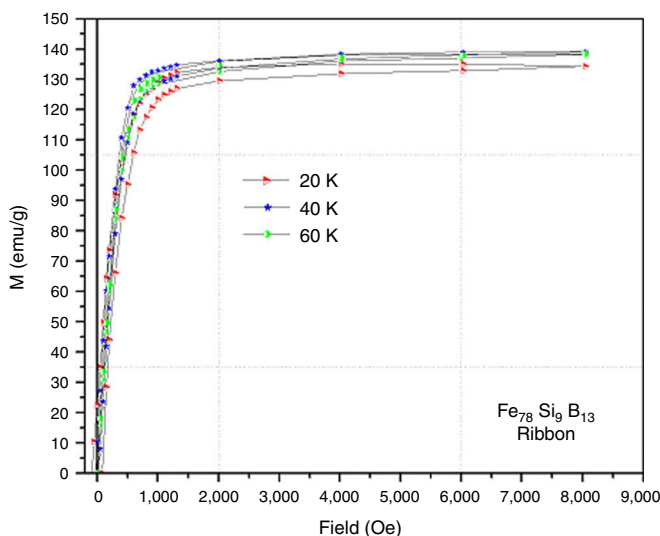
Figure 8.
Magnetic response
analysis (first quadrant)
of $Fe_{78}Si_9B_{13}$ (%at.)
study ribbon

function around crystalline diffraction patterns in the analogous diffractogram (Figure 5 – ingot and TT Ribbon). This occurs due that the same material chemical composition is studied in both cases. Furthermore, the ribbon production route promotes the metastable states formation in the sample. These results show amorphization in the described XRD peaks in Section 3.2.

The difficulty when analyzing by Transmission Electron Microscopy is due to the obtained average thickness of the ribbons (Ribbon and TT Ribbon) since the recommended thickness lm is limited to few hundreds of nanometers in this technique (Busby and Pireaus, 2014). This do not allow us to supplement DSC studies. However, the results obtained in both first and second transformation, as in Curie Temperature are consistent with studies by other authors in similar materials, as shown in the bibliography of Section 3.3.

The DSC ribbons results show the first crystallization (T_{Fc}) (see Figure 6) than the amorphous regions rich in Si and B as determined by XRD (Figure 5 – Ribbon) after the heat treatment gave rise to a nanocrystalline iron-silicon solid solution α(Fe Si) ($Fe_{0.91}Si_{0.09}$ (Nc)) with a cubic structure (Thongmee S. et al., 2009; Chacón et al., 2001). With a random orientation of the nanoscale grains is attributed to reduction in the net magneto-crystalline anisotropy, resulting in high permeability (Herzer, 1989). Using a heat treatment increases the number of nanocrystals. The dimensions are reported in Table V.

Considering the impurities in the noncommercial scrap alloys: Al, C, Ca and S are lower than 0.3 %wt., we obtain a sample with the desired atomic composition $Fe_{78}Si_9B_{13}$ observed in Equation (3). Such impurities are not able to form detectable phases by the used techniques in the work.

3.7 Specific discussions

• The EDS results at center and surface ingot (Figure 4) confirms a Fe uniform distribution in volume, the obtaining values of 91.7 (%wt.) are comparable with the proposal starting alloy (Equation (3)).

- The XRD ingot results shown crystalline structure in all peaks obtained (Figure 5 – ingot) which in conjunction with the stoichiometry of the starting alloy (Equation (3)) show the appearance of Fe_2B (C) and $FeSi_2$ (C) and Fe (C) according to cards #39-1314; #35-0822 and #06-0696 (see Table IV).

- The XRD ribbon results shown a mostly amorphous structure (Am) in the peaks obtained (Figure 5 – Ribbon) which in conjunction with the stoichiometry of the starting alloy (Equation (3)) produces the majority appearance of $Fe_{0.91}$ $Si_{0.09}$ (Am) phase and FeB (Am) and Silicon boride SiB_6 (Nc) minority of size 3.260 nm, according to cards #96 – 900-6909; #32-0463 and #35-0809, respectively (see Table IV).

- The treated ribbon XRD results show a majority nanocrystalline structure (Nc) in the peaks obtained (Figure 5 – TT Ribbon) which in conjunction with the stoichiometry of the starting alloy (Equation (3)) show the appearance of $Fe_{0.91}Si_{0.09}$ (Nc) phase, $FeSi_2$ (Nc) and B_β (Nc) of specified sizes in Table IV, according to the cards #96 – 900-6909, #35-0822 and #31-0207 (see Table IV).

- The MS analysis confirms the suggested by Miglierini (1994) and Franke et al. (1980) for Fe atoms environments surrounded Si and FeB rich environments, respectively. The same amorphous phases are nanocrystalline solutions precursors determined by XRD (see Figure 5 – TT Ribbon).

- Magnetic analysis confirmed that $Fe_{78}Si_9B_{13}$ (%at.) alloy in ribbon form after being processed by the technique of melt spinning is magnetically soft and does not vary substantially its saturation value (135 emu/g) in the tested temperature range (20-80 K) (see Figure 8). While the coercivity and remanence decrease with increasing temperature as reported in Section 3.5.

4. Conclusions

As a general conclusion we can say that this proposed route has achieved a soft magnetic ribbon (product) designed with noncommercial scrap alloys. These materials may compete with those produced by conventional casting processes. In addition, we can improve the efficiency achieved, obtaining predominantly a nanocrystalline phase, with posterior heat treating, with the advantages in the performance that this entails.

This process achieved a production with lower cost, high efficient energy products and high added value.

References

Allia, P., Ferro Milone, A., Vinai, F., Fratucello, G. and Ronconi, F. (1982), "Mössbauer spectroscopy of amorphous Fe-Si-B alloys with different free volume content", *Journal of Applied Physics*, Vol. 53, pp. 7750-7753.

Aykol, M., Mekhrabov, A.O. and Akdeniz, M. (2009), "Nano-scale phase separation in amorphous Fe-B alloys: atomic and cluster ordering", *Acta Mater*, Vol. 57 No. 1, pp. 171-181.

Bedell, J.R., Hemmat, N.S. and Jeges, P. (1987), "Method of and apparatus for casting metal strip employing a localized conditioning shoe", *US Patent*, Vol. 4, pp. 649-984.

Busby, Y. and Pireaux, J.J. (2014), "Metal nanoparticle size distribution in hybrid organic/inorganic films determined by high resolution X-ray photoelectron spectroscopy", *Journal of Electron Spectroscopy and Related Phenomena*, Vol. 192, pp. 13-18.

Byoung-Gi, M., Yong Sohn, K., Won Wook, P. and Taek Dong, L. (2007), "Effect of milling on the soft magnetic behavior of nanocrystalline alloy cores", *Materials Science and Engineering A*, Vols 426/449, pp. 449-451, doi: 10.1016/j.msea.2005.12.103.

Calvert, L. (1985), *National Research Council of Canada*, ICDD, Ottawa.

Chacón, J.O., Rosales Rivera, A., Minotas Ruiz, J. and Echavarría Velásquez, A. (2001), "Mecanismo de desvitrificación no-isotérmica de una aleación vítrea, magnéticamente blanda, $Fe_{0.75}Si_{0.15}B_{0.10}$", *Revista Colombiana de Materiales*, Universidad de Antioquia, Facultad de Ingeniería, ISSN 2256-1013, pp. 80-95.

Chang, C.F. and Marti, J. (1983), "Crystallization of the metallic glass $Fe_{80}B_{12}Si_8$", *Journal of Materials Science*, Vol. 18 No. 8, pp. 2297-2304.

Chau, N., Hoa, N.Q. and Luong, N.H. (2005), "The crystallization in Finemet with Cu substituted by Ag", *Journal of Magnetism and Magnetic Materials*, Vols 290/229, pp. 1547-1550.

Chen, Z., Lei, Y. and Zhang, H. (2011), "Structure and properties of nanostructured A357 alloy produced by melt spinning compared with direct chill ingot", *Journal of Alloys and Compounds*, Vol. 509 No. 27, pp 7473-7477.

De Cristofaro, N. (1998), "Amorphous metals in electric power distribution applications", *Materials Research Society, MRS Bulletin*, Vol. 23 No. 5, pp. 50-56.

Dobrzanskia, L.A., Nowosielskia, R., Koniecznya, J., WysŁockib, J. and PrzybyŁb, A. (2004), "Properties and structure of the toroidal magnetically soft cores made from the amorphous strips, powder, and composite materials", *Journal of Materials Processing Technology*, Vols 157/158, pp. 669-678.

Franke, H. (1980), "Hyperfine fields and local magnetic moments of metallic glasses of 3d-transition metals", *Journal of Magnetism and Magnetic Materials*, Vols 15/18, pp. 1364-1366.

Gelinas, C. (2000), *Soft magnetic Powders for AC Magnetic Applications*, Euro PM2000, Soft Magnetic Materials Workshop, Berlin, pp. 1-8.

Herzer, G. (1989), "Grain structure and magnetism of nanocrystalline ferromagnets", *IEEE Trans Mag Magn*, Vol. 25 No. 5, pp. 3327-3329.

Khan, Y. (1988), *Institut. Werkstoffe Elektrotechnik*, Queremburg, Bochum.

Khorsand Zaka, A., Abd Majida, W.H., Ebrahimizadeh Abrishami, M., Ramin, Y. and Parvizi, R. (2012), "Synthesis, magnetic properties and X-ray analysis of Zn0.97X0.03O nanoparticles (X 1/4; Mn, Ni, and Co) using Scherrer and sizeestrain plot methods", *Solid State Sciences*, Vol. 14 No. 4, pp. 488-494.

Kim, D.H., Kim, W.T., Park, E.S., Mattern, N. and Eckert, J. (2013), "Phase separation in metallic glasses", *Progress in Materials Science*, Vol. 58 No. 8, pp. 1103-1172.

Kurokawa, K., Suhara, S., Matsukawa, T., Ishizuka, H. and Sato, T. (1999), "Method of manufacturing a wide metal thin strip", *US Patent*, Vol. 5, pp. 908-068.

Lavorato, G.C., Marta, L., Moya, J.A. and Pagnola, M. (2011), "Análisis de parámetros experimentales para modelado de diámetros máximos en piezas cilíndricas de amorfos estructurales base Fe", Tercer Simposio en Mecánica de Materiales y Estructuras Continuas: SMEC 2011, 18, 19 y 20 de Octubre de 2011,Cartagena de Indias, Colombia, pp. 1-10.

Lim, K.M., Lee, K.A., Kim, O.S., Hong, Y.M. and Park, C.G. (2009), "Magnetic properties of amorphous alloy strips fabricated by planar flow casting (PFC)", *Journal of Physics: Conference Series*, Vol. 144 No. 1, pp. 1-4.

Miglierini, M. (1994), "Mossbauer-effect study of the hyperfine field distributions in the residual amorphous phase of Fe-Cu-Nb-Si-B nanocrystalline alloys", *J. Phys.: Condens. Matter*, Vol. 6 No. 7, pp. 1431-1438.

Muraca, D., Silveyra, J., Pagnola, M. and Cremaschi, M. (2009), "Nanocrystals magnetic contribution to FINEMET type soft magnetic materials with Ge addition", *Journal of Magnetism and Magnetic Materials*, Vol. 321 No. 21, pp. 3640-3645.

Natl. Bur. Stand (US) (1981), "Monogr", Vol. 25, October, pp. 18-35.

Natl. Bur. Stand (US) (1984), "Monogr", Vol. 25 No. 20, pp. 21-45.

Natl. Bur. Stand (US) (1985), "Monogr", Vol. 25 No. 21, pp. 21-73.

Nowacki, J. (2006), "Polyphase sintering and properties of metal matrix composites", *Journal of Materials Processing Technology*, Vol. 175 No. 1, pp. 316-323.

Olofinjana, A.O., Kern, J.H. and Davies, H.A. (2004), "Effects of process variables on the multi-strand casting of high strength sub-millimetre metallic glass wire", *Journal of Materials Processing Technology*, Vols 155/156, pp. 1344-1349.

Pagnola, M. and Katabian, R. (2012), "Development of a winding mechanism for amorphous ribbon used in transformer cores", in Gokcek M. (Ed.), *Mechanical Engineering*, ISBN 978-953-51-0505-3, Chapter 12, InTech, pp. 277-291.

Pagnola, M., Saccone, F., Ozols, A. and Sirkin, H. (2009), "Improvement to approximation of second order function of hysteresis in magnetic materials", *COMPEL: The International Journal for Computation and Mathematics in Electrical and Electronic Engineering*, Vol. 28 No. 6, pp. 1579-1589.

Pavuna, D. (1981), "Production of metallic glass ribbons by the chill-block melt spinning technique in stabilized laboratory conditions", *Journal of Materials Science*, Vol. 16 No. 9, pp. 2419-2433.

Praisner, T., Chen, J. and Tseng, A. (1995), "An experimental study of process behavior in planar flow melt spinning", *Metallurgical and Materials Transactions B*, Vol. 26B No. 1, pp. 1199-1208.

Rawers, J.C., McCune, R.A. and Adams, A. (1988), "Cristallyzation of amorphous $Fe_{78}B_{13}Si_9$ alloys", *J. Mater.Sci. Lett.*, Vol. 7, pp. 958-960.

SGTE (2004), "B-Fe Alloy phase diagrams (Revised)", available at: www.crct.polymtl.ca/FACT/phase_diagram.php?file = B-Fe.jpg&dir = SGTE

Sun, X., Cabral-Prieto, A., Yacamn, M.J., Reyes-Gasga, J., Hernandez-reyes, R., Morales, A. and Wensheng, S. (2000), "Nanocrystallization behavior and magnetic properties of amorphous $Fe_{78}Si_9B_{13}$ ribbons", *Physica B*, Vol. 291 Nos 1/2, pp. 173-179.

Švec, P., Krištiaková, K. and Deanko, M. (2003), "Cluster structure of the amorphous state and (NANO) crystallization of rapidly quenched iron and cobalt based systems", *Nanostructures: Synthesis, Functional Properties and Applications NATO Science Series*, Vol. 128, pp 271-294.

Swanson, H.E., Fuyat, R.K. and Ugrinic, G.M. (1955), "Natl. Bur. Stand (US)", Circ. 539, pp. 3-4.

Thongmee, S., Issro, C., Roongkeadsakoon, S., Winotai, P. and Tang, I.M. (1999), "Nanocrystalline formation in Amorphous $Fe_{79}B_{16}Si_5$ and $Fe_{78}B_{13}Si_9$ ribbons", *Mod. Phys. Lett. B*, Vol. 13 Nos 6/7, pp. 175-179.

Wang, C. (2010), "Numerical modeling of free surface and rapid solidification for simulation and analysis of melt spinnnig", *Iowa State University, Ames Ed.*, ProQuest, UMI Dissertation Publishing, ISBN 10: 1243778733/1-243-77873-3, pp. 1-138.

Yardley, V.A., Tsurekawa, S., Fujii, H. and Matsuzaki, T. (2007), "Thermodynamic study of magnetic field-enhanced nanocrystallisation in amorphous Fe-Si-B(-Nb-Cu)", *Materials Transactions*, Vol. 48 No. 11, pp. 2826-2832.

Yoshizawa, Y., Oguma, S. and Yamauchi, K. (1988), "New Fe-based soft magnetic alloys composed of ultrafine grain structure", *Journal of Applied Physics*, Vol. 64 No. 10, pp. 6044-6047.

Zhang, J. and Guyot, F. (1999), "Thermal equation of state of iron and $Fe_{0.91}Si_{0.09}$", *Physics and Chemistry of Minerals*, Vol. 26 No. 3, pp. 206-211.

Corresponding author
Dr Marcelo R. Pagnola can be contacted at: mpagnola@gmail.com